3.7. Arc Jet Test Facilities[1]

Among all the ground test facilities that have been developed over the past 7 decades for testing TPS, arc jet ranks as the most flight relevant and extensively used test facility in the history of TPS development in the US. Arc Jet facilities played, and continue to play, a critical role not only in the early screening and selection of TPS materials, but more importantly, in the flight vehicle integrated development and in the flight qualification.

3.7.1. Introduction and historical background

In the late 1950's, researchers in the US, for the first time, realized that the hypersonic re-entry required solving the re-entry heating associated with deceleration [65]. Attempts to design supersonic X-planes, hypersonic missiles, and re-entry systems for missions to Moon, Mars, and Venus by NACA (which became NASA in 1959) required developing insight into re-entry heating [66, 67]. The desire to develop a series of successful flight vehicles, first orbiting around earth and then around Moon, and safely returning astronauts back to Earth required development of relevant ground test facilities so that the thermal protection materials and system could be designed with mission success in mind. Experience with sharp body flight tests led to the realization that metals and coatings are not the solution for hypersonic re-entry and in order to be successful, re-entry shapes need to be blunt [68]. The aerothermodynamic flow around blunt bodies were studied using ballistic range and shock tunnels, but these facilities were not suitable for thermal protection materials screening or development. Early attempts to use flight testing were expensive and provided limited insight [67] [69]. In the mid 1950's, arc jet facilities were beginning to be designed in the US, based on World War II German design. The earliest picture of an arc jet test, an X-ray image of the posttest article obtained in 1958 highlighted by G. W. Sutton in his historical keynote address [70] is reproduced in Figure 3.17.

Fig. 3.17. The above figure from Ref [70] shows one of the earliest (1958) ablative TPS, silica-phenolic, post-test article tested in the arc jet by the Chicago Midway Laboratories. One can observe the tape wrapped material from the x-ray image and also the threaded screw at the bottom.

---

[1] The material in this section is declared the work of the U.S. Government and is not subject to copy right protection in the United States. This section was written by Dr. Ethiraj Venkatapathy, NASA Senior Technologist for Entry Systems, NASA Ames Research Center, Moffett Field, CA.

Variant of silica-phenolic ablative TPS materials were used later in DoD ballistic missiles and on NASA's Mercury mission.

Mercury, Gemini, and Apollo missions all used ablative TPS. Arc Jet testing became essential for ablative material screening and development in the late 1950's and early 1960's. Many organizations in the late 50's and early 60's, private and public, designed, built and used arc jets to support a variety of missions in support of both the civilian and military programs. During the Apollo era, the challenge of reaching the Moon within the decade meant extensive flight testing. For each flight test program to be successful, extensive testing was required. There was not a single mission failure due to ablative TPS during the Mercury, Gemini, and Apollo programs. Apollo programs success can directly be attributable to the extensive arc jet testing. The number of arc jets as well as their uses in the 1960's were phenomenal. This was driven by the need during that period to develop intercontinental ballistic missiles as well as to the Apollo program [71].

Figure 3.18 shows only a small number of arc jets relative to the many that were available at that time. The number of tests performed in the development of Apollo TPS exceeded 10,000. It also shows the variety of tests performed, not just material test but included TPS system integration relevant tests as well. The figure shows the use of arc jets in the screening of TPS to in the development and flight certification of TPS for Mercury, Gemini, and Apollo programs from 1960 – 1969. During the late 1950's GE, AVCO, Chicago Midway, Plasmadyne, Rocketdyne, Boeing, NASA MSC, NASA LaRC, and NASA Ames all had their own arc jets.

Figure 3.18. More than 10,000 arc jet tests were performed across a variety of arc jets located across the US in the development of TPS for the Apollo program [71].

Termination of the Apollo program impacted the number of arc jet facilities around the country and many of the facilities were closed due to lack of use. NASA facilities were consolidated into two locations. The NASA JSC arc jet facility became the primary facility devoted to Space Shuttle Orbiter TPS testing and NASA Ames arc jet facility became the primary facility for planetary missions. This did not diminish the importance or the use of the arc jet in

TPS development and certification. Space Shuttle Orbiter development and flight certification required equally large number of arc jet tests similar to the Apollo program. Space Shuttle Orbiter program decided to forgo any flight test prior to the first manned flight unlike Apollo and one can attribute this to the confidence gained through arc jet testing of a variety of Space Shuttle Orbiter reusable TPS materials.

Figure 3.19 shows all of the NASA missions over the past 7 decades that required TPS. The termination of the Space Shuttle Program led to further consolidation. NASA relocated the JSC arc jet facility to NASA Ames after the Space Shuttle program. Today NASA Ames' arc jet complex has become the major facility in the nation for TPS flight qualification testing in support of NASA missions such as Orion, Commercial Crew Vehicles, Mars 2020, Dragonfly, and other planetary missions. Two other facilities, HYMET facility at NASA LaRC, VA, and the other, the Boeing LCAT facility in St. Louis are used for TPS material development testing. Similarly, on the Department of Defense side, over the years, consolidation has led to single major arc jet test facility, namely Arnold Engineering Development Center (AEDC) in Tennessee.

Fig. 3.19. NASA Missions, from the 60's through present, that utilized arc jet in their TPS development (Courtesy of NASA Ames Research Center).

3.7.2. Arc Jet

An arc jet is a high-temperature wind tunnel. An electric arc, anchored between an anode and a cathode, heats the high pressure and nearly stagnant gas to a high-temperature, high pressure plasma. The heated gas is then expanded through a convergent-divergent nozzle to supersonic jet (Figure 3.20). When a small test article is introduced into the jet, the conditions generated behind the shock wave on the test article are similar to re-entry conditions on a spacecraft. By varying the electrical power and the mass flow rate, the energy density (or enthalpy) of the gas stream and the surface heat flux and the pressure on the test article can be varied for performing test to match required flight like conditions.

The arc heaters are key features of the arc jet complex; they contain three fundamental elements: a cylindrical volume for containment of the arc discharge (or arc), a pair of electrodes (anode and cathode), and a nozzle [72]. The desired test gas is injected into the cylindrical section

and an arc discharge passes between the electrodes, heating the gas to a high temperature. The plasma then flows through a converging/diverging supersonic nozzle, producing the simulated atmospheric-entry heating environment. The design of the cylindrical confining device must simultaneously satisfy numerous difficult requirements. The confining device must incrementally withstand the voltage potential between the electrodes, which can total more than 20,000 volts (V). It must be highly water cooled in order to contain the plasma, which can reach temperatures in excess of 15,000°F (8,300°C). It must serve as a pressure-containment vessel; as such, all seals and joints must be adequate to prevent leakage at conditions ranging from vacuum up to pressure levels of several hundred pounds per square inch (psi). It must have adequate mechanical strength for the loads involved. Finally, the materials used must have the proper electrical, thermal, mechanical, and chemical properties to meet all of these requirements.

Figure 3.20. A schematic of the 60 MW segmented arc jet used in the Interacting Heating Facility (IHF) at NASA Ames Research Center [73].

In contrast to the segmented arc heater, the Huels type, arc heater [74], shown in Fig. 3.21, is much simpler to design and operate. But they do not provide consistent test condition as the arc attachment point and the arc column length are difficult to control and the conditions can vary during the testing.

Figure 3.21. Schematic of Huels arc heater design used in the H2 facility at AEDC [74].

Stability of the arc column, and control of the arc attachment points on the electrodes is essential in order to maintain thermal-structural survivability of the plenum, optimum heat transfer to the gas, and sustained electrical integrity of the arc discharge. Consequently, arc heaters are commonly classified by the method used to stabilize the arc discharge within the chamber.

There are three primary types [75]. They are vortex stabilized arc heater such as Huels, which uses a strong swirl inside the arc chamber to provide arc stability. Another type is magnetically stabilized arc heater where stability of the arc column is maintained by means of external magnetic coils placed around the heater plenum, which rotate the arc termination on the chamber wall. The third category is a hybrid with respect to arc stabilization mode, typically utilizing vortex and

magnetic stabilization of the arc, along with segmented construction to efficiently produce a clean, superheated test gas. The widespread utilization of the modern segmented arc results from significant practical advantages inherent in the design which optimize performance of the heater as a generator of non-vitiated high-enthalpy gas test flows. Arc Jets can be operated up to an hour duration depending on the conditions. They are unique in that they not only provide high-temperature gas at relevant conditions (Figure 3.22) but also longer duration testing necessary for TPS development and flight certification.

Figure 3.22. Comparison of high-temperature test facilities in terms of stagnation temperature and test duration [73].

In the US, there are only three arc jet complexes that can support TPS development and certification. These capabilities were designed and developed with certain class of missions in mind. Hence, the capabilities they provide are distinct with some limited overlap.

1. Ames Research Center Arc Jet Complex [72]:
    a. 60 MW Interaction Heating Facility (IHF)
    b. 20 MW Aerodynamic Heating Facility (AHF)
    c. 20 MW Panel Test Facility (PTF) [includes the Truncated-PTF (TPTF)]
    d. 12 MW (2” x 9”) Turbulent Flow Duct (TFD)
    e. 10 MW TP-3 (moved from JSC as a result of consolidation)
    f. The Laser Enhanced Arc jet Facility (LEAF-Lite) in combination with IHF can provide both convective and radiative heating by the use of multiple 50-kW CW lasers.
2. Arnold Engineering Development Center Arc Jet Complex [76]:
    a. 30 MW High Enthalpy Ablation Test Unit H1 (HEAT-H1)
    b. 45 MW HEAT-H2
    c. 70 MW HEAT-H3
3. Boeing Large Core Arc Tunnel (LCAT) 12 MW Arc Jet Facility (St. Louis) [73].
4. 400 kW Hypersonic Materials Environmental Test System (HyMETS) arc jet facility [77] at NASA Langley Research Center used primarily for material characterization of ceramic matrix composite (CMC) materials, rigid and flexible ablators, high-temperature coatings, and for performing research and development on plasma flow diagnostics.

One way to compare arc jet operational envelope is to compare the arc heater capability in terms of pressure and enthalpy (velocity) achievable with relevant missions. Figure 3.23 shows an altitude (= pressure) and velocity (= enthalpy) map of different missions and compare these to the performance envelopes of the different facilities. AEDC arc jet test facilities were primarily designed to produce test conditions relevant for ICBM and hence they operate at conditions that simulate heating at higher pressure and lower velocity (lower enthalpy). NASA facilities were designed with Apollo (Lunar return) and Space Shuttle Orbiter missions in mind and hence they operate at higher altitude (lower pressure) and higher velocity (higher enthalpy). The LCAT facility provides conditions that are comparable to that of NASA facility with a 12 MW Hules type heater and hence it can test smaller test article compared to NASA arc jet.

Figure 3.23. Re-entry trajectory and the peak heating conditions for ICBM, Space Shuttle Orbiter, Apollo, Mars, and Far Solar System missions are compared to the NASA Ames, Boeing LCAT, and AEDC arc jet complex operational envelope [73].

The AEDC H2 facility does have a region of interest for NASA missions: it captures a portion of the Apollo (CEV), Mars return, and far solar system return trajectories. But the peak heating conditions of Mars direct return or far solar system return conditions, identified as red dots, are beyond the capabilities of existing facilities.

The maximum arc heater power (current and volated) capability combined with the gas injection mass flow rate can be adjusted to achieve a range of conditions in the constrictor section which then can be expanded to provide flexibility in test condition by the use of nozzles. But the primary control is the arc heater setting. Increasing power for a given mass flow rate, increases the enthalpy and pressure and thus provides higher heat flux test capability. For a given power setting, increasing the mass flow rate lowers the enthalpy but increases the pressure. For NASA missions, both human and robotic, high enthalpy and high heat flux are desired as the re-entry happens at much higher speed and the deceleration happens at higher altitude and hence at relatively lower pressure. For DoD applications, desired flight conditions are at much higher pressure and lower velocity. This means DoD missions are at lower enthalpy but much higher pressure. Hence, the mass flow rate for the DoD are much higher to achieve higher pressure.

Arc Jet operations require substantial infrastructure in order to not only produce high-

temperature test conditions but also for long duration operations (Figure 3.24). DC power supplies, de-ionized cooling water system, high-pressure gas systems, data acquisition system, steam ejector vacuum system for creating very low pressure in the test section, and other auxiliary systems are all required for its control and safe operations. For example, the NASA Ames Arc Jet Complex has access to a very large DC power supply that can deliver 75 MW for 30 minutes. High-power capability, in combination with the high-volume steam-ejector vacuum system, and high pressure de-ionized cooling water system yields a unique suite of facilities that simulate high-altitude atmospheric flight on relatively large test objects.

Figure 3.24. NASA Ames Arc Jet Complex, supported by a common infrastructure that occupied (2 – 3) city block, consists of Aerodynamic Heating Facility (AHF), Interaction Heating Facility (IFH)), Panel Test Facility (PTF), and Turbulent Facility (TFD) [72].

In order to conduct a successful arc jet test, the conditions desired should be achievable in the arc jet. The arc jet operational envelope is determined by many factors. First, it starts with the arc heater itself. It has limitations due to electrical power and mass flow rate of the gas that can be introduced into the arc column, the operational pressure of the constrictor and the cooling water pumping rate. Each facility mentioned above uses a variety of nozzles to expand the core flow to provide a range of test conditions. For a given arc heater setting, test conditions achievable can be modified by the nozzle geometry. The nozzle is often designed in segmented manner so as to achieve some flexibility (Figure 3.25). The nozzles constructed in modular/segmented fashion can modify the exit jet conditions. The size of the jet limits the size of the test article. In addition to the nozzle segments, the jet can be expanded further. The test bay or cabin pressure also determines how fast or slow the jet exiting the nozzle may expand. By maintaining the test cabin pressure very low, by the use of the vacuum system connected to the test cabin, as the case at NASA ARC facilities as well as in the AEDC H2 facility, the nozzle jet flow is over-expanded and thus larger than nozzle exit diameter test article can be tested. In the case of AEDC H1 and H3 facility, the nozzle exhausts into atmospheric conditions with a perfectly expanded jet and the test article size is nearly equal to the nozzle exit diameter. The nozzles segments do not have to be axisymmetric (Figure 3.26). Though the first nozzle segment is axisymmetric, since the arc heater core is axisymmetric, the subsequent sections can be designed so that the nozzle transitions from an

axisymmetric throat to desired exit geometry.

Figure 3.25. Nozzle extensions are often used to expand the flow from to achieve lower test condition with larger test articles in a given arc jet facility [72].

Figure 3.26. Schematic Drawing of a semielliptical nozzle used at NASA ARC [72].

The combination of segmented nozzles and control over arc heater setting provide a range of test conditions. The range of facility operating conditions for the NASA Ames arc jet complex are given in Table 3.5 and at AEDC in Table 3.6.

Table 3.5. *NASA Ames Arc Jet Test Facilities Conditions [78]*

Table 3.6. *AEDC Arc Jet Test Facilities Conditions [79]*

3.6.3 Test Condition in the Arc Jet

As the name implies, arc heated jet in the test section is generated by accelerating the plasma gas in the arc column through a convergent-divergent nozzle to reach hypersonic speeds at the exit of the nozzle. The test article will be introduced in the test section some finite distance downstream of the nozzle exit. For a given arc heater setting and the nozzle configuration, the test conditions can vary depending on the location of the model, nozzle shape, and the pressure of the test cabin. The expansion of the jet, exiting the nozzle, is impacted by the cabin pressure. Typically, the test article for TPS testing is either a blunt-body or a wedge. The test article produces a shock wave that compresses the flow and modifies the conditions. The conditions that are relevant are the post-shock conditions, which the test article is exposed to. In order to determine the post shock conditions, conditions ahead of the shock are needed. Hence, it is necessary to know how ascertain conditions at the location of the testing without the test article first and then determine the conditions that the TPS test article will experience.

Figure 3.27. A simplified view of the relationship between flight and facility.

To relate the test conditions to flight condition, it is necessary to understand that the state and the composition of the gas that the flight article surface is exposed to are also

the post-shock conditions during entry. In a simplified manner this is illustrated in Figure 3.27. What relates the flight to facility are the post-shock conditions. These may include stagnation pressure, thermo-chemical state of the gas including temperature(s), composition of the gas and enthalpy. The post-shock conditions cannot be determined without knowing the conditions upstream of the shock whether in the facility or in flight. The key parameter in arc jet testing is specific total enthalpy (H), especially since this is conserved across a normal shock (i.e., the flow is adiabatic across the shock front) [80]. Specific total enthalpy is a sum of three components—the internal part, the chemical part, and the kinetic part, *i.e.*,

$$H = \overbrace{\underbrace{\sum_{s=1}^{n_s} c_s h_s(T)}_{\text{Internal}} + \underbrace{\sum_{s=1}^{n_s} c_s\left(\Delta_f^o h_s\right)}_{\text{Chemical}}}^{\text{Static}} + \overbrace{\frac{1}{2}V^2}^{\text{Kinetic}}$$

where c_s is the mass fraction of species s, h_s is the standard enthalpy of formation, and V is the velocity.

For the flight case, the kinetic part of the total enthalpy dominates the other two because: (i) the freestream temperature is quite low and (ii) the chemical component of static enthalpy is usually zero—for Earth entries, N_2 and O_2 have a standard enthalpy of formation of zero by definition. However, the chemical component is non-zero for entries into the Mars and Titan atmospheres—CO_2 in the Mars atmosphere has a chemical enthalpy of formation of -8.9 MJ/kg, and the small amount of CH_4 in the atmosphere of Titan has a formation enthalpy of -4.2 MJ/kg [80].

In the arc jet, total enthalpy is a measure of the energy in the stream. Enthalpy allows the facility conditions to be relatable to flight. In an arc-heated stream, the flow velocity (hence the flow kinetic energy) is smaller than flight, but the atomic species in the dissociated gas mixture add to the chemical portion of static enthalpy. Furthermore, the vibrational temperature freezes (at a high level) upon expansion in the nozzle and adds to the internal part of static enthalpy. The two contributions raise the total enthalpy to flight-like levels. For a typical working medium, such as air, the standard enthalpies of formation of N_2 and O_2 are zero (by definition). However, the standard enthalpies of formation of N and O are 33.6 MJ/kg and 15.4 MJ/kg, respectively. If the

23% (by mass) of molecular oxygen in air is completely dissociated, the chemical content of the gas could be increased by as much as 3.6 MJ/kg from atomic oxygen alone [80].

In the case of arc jet flow, the enthalpy varies (Figure 3.28) from the stagnation (highest) value in the arc column to a much lower value in the test section as a result of acceleration and the changing thermo-chemical state throughout the expansion.

Figure 3.28. The center-line enthalpy and the pressure profile.

Since the total (or stagnation) enthalpy does not change through the shock, if it can be inferred from measurable quantities, then it is easy to relate facility post-shock conditions to the flight post-shock conditions. The primary method of determining test conditions has been to directly survey the region by measuring the stagnation point heat-transfer, pitot pressure and then relate it to the total enthalpy. With certain assumptions the total stream enthalpy can be inferred from a simultaneous measurement of heat transfer and impact pressure at the stagnation point of a blunt-body, such as a sphere or cylinder using empirical correlation [81-83].

$$h = \frac{q}{\kappa}\sqrt{R\text{eff}/Pp}$$

where *k* is a gas species dependent constant, q is the stagnation point heat flux, R_{eff} is the effective radius of the blunt-body, Pp is the total pressure, and Δ is the difference between the stream and cold wall enthalpy. A clear advantage of this approach is that it gives a spatially resolved measure of the stream enthalpy at the location of the heat flux and pressure measurements.

It is a common practice to perform facility characterization across the jet at a desired location downstream of the nozzle exit with both pitot pressure and null point calorimeter sweeps to determine the variation of the enthalpy across the jet. In addition, slug calorimeters are used to measure center line pressure and heat flux typically with every test series (Figure 3.29). Such a survey provides a measure of the core flow diameter and also provides the inherent variability within the core.

Figure 3.29. Standard calorimeters, (a) Hemi-sphere, (b) Iso-q, (c) Flat-face cylinders and

(d) Null point calorimeters. A small copper slug (or Gardon gauge) is located at the center of each of the first three oxygen free copper calorimeters. The null point calorimeter has a very small (and quick time response) heat-sensing element at the tip of the hemisphere-cone body made of oxygen free copper. The sensing element of the null point calorimeter is actually flat [80].

Figures 3.30 and 3.31 are from [80], show survey results for the NASA ARC AHF and IH, respectively in terms of radial variation.

Figure 3.30. Profiles of heat flux and pitot pressure obtained by sweeping 5/8-inch hemisphere-cylinder probes across the jet of the AHF 18-inch axisymmetric nozzle for various arc-heater conditions. The probes were swept at an axial location of 10 inches from the nozzle exit plane. The pitot pressure and heat flux traces show small variations in what can otherwise be considered an uniform distribution (Figures and caption from [80]).

Figure 3.31. Profiles of heat flux and pitot pressure obtained by sweeping a null point calorimeter, and a 5/8-inch hemisphere-cylinder probe, respectively, across the jet of the IHF 6-inch nozzle for various arc-heater conditions. The probes were swept at an axial location of 3 inches from the nozzle exit plane. While the pitot pressure traces show essentially uniform pressure across the jet, the heat flux traces show distinct profiles. Assuming the effective radius of the null point probe does not vary across the jet, one can conclude that profiles of total enthalpy have the same shape as the heat flux. (Figure and caption from [80]).

The variations in the measurements are informative for two reasons. The variations in enthalpy in the radial direction need to be taken into account in test design as well as interpreting the results. These profiles indicate the core of the flow is smaller than the nozzle diameter. Hence the model size will need to be limited and the model design needs to take into account the size of the core region at the location where the model will be

tested.

It is not easy to measure the chemical and thermal state of the gas either ahead of the shock or near the surface of the test article. Laser diagnostic and emission spectroscopic techniques have been used with limited success, but they do not fully define the state [84]. It should be noted that arc jet testing cannot match all of the flight parameters. In addition, arc jets have limited capability to test with right gas composition. Air and N_2 are more prevalent than CO_2 test gas and the test facility that was H_2/He gas for testing TPS for the Galileo probe no longer exist. As a result of these limitations, the test conditions typically are selected based on matching heat flux and pressure at relevant enthalpy. With different size nozzle and the ability to control mass flow, current and voltage in the arc column, the facility test envelope is described in terms of heat flux and pressure with respect to a reference geometry (slug calorimeter). Figure 3.32, taken from [72], illustrates this.

Figure 3.32. Operating envelope of the AHF with 20-MW segmented arc heater [72].

In addition to the conical nozzles, some facilities use semi-elliptic nozzles where the test article is typically a flat plate configuration mounted on the wall and takes advantage of the wall boundary layer for shear dominated flow. Inserting and keeping the model in the jet is not a trivial effort as there is significant mechanical and thermal load imparted to the model and the sting arm holding the model. The model holder along with the sting need to be strong and parts of it need to be water cooled. Each arc jet test facility has a unique way of introducing the model into the flow. In Figure 3.33, taken from [72], a water-cooled model holder cut-away view along with pictures of the 5 sting arms in the AHF and one of the two sting arms in the IHF are shown.

Figure 3.33. The test article model holder and the typical test set-up in NASA's AHF and IHF arc jet facilities.

Not all testing is done with stagnation test coupons. A wedge configuration (Figure 3.34) allows for boundary layer to develop and provide effect of boundary layer including shear [85, 86]. Depending on the conditions, the boundary layer may be laminar or turbulent. Compared to

stagnation article, wedge tests typically provide lower pressure and heat flux compared to a stagnation test at the same arc jet setting as the flow is expanded from the stagnation to the wedge surface.

Figure 3.34. An example of a wedge test article used in early Crew Exploration Vehicle (CEV) and in MSL TPS testing [85].

Designing test articles, whether they are stagnation or wedge, is an involved process and requires a good understanding of facility capability, operations and limitations as well as a clearly defined test objective. The integration of the model holder with the sting, selecting the right size and shape of the test article, the data to be collected during the test, such as imbedded thermo-couples or surface temperature, and post-test measurements and analysis all require complex pre-test analysis. In terms of data collection, arc jet facilities provide some measurements as standard practice and the feasibility of novel data collection have to be explored in consultation with the facility operators. Most arc jet facilities measure and provide heat flux and pressure measurement at the test section using calorimeters, and surface temperature using pyrometers, IR cameras, high speed video and photographs are also standard in most facilities. It is standard practice to collect data from thermocouple plugs imbedded within test articles using the facility data acquisition system. In some facilities, IHF and AHF, laser induced fluorescence (LIF) measurement could be requested with or without the model. Also, photogrammetric recession measurement (PRM) is an optical technique to provide a time history of recession of an arbitrary number of points on the surface and could be deployed as an optional measurement [72].

3.7.4 Facility to Flight and Test Design

Relating flight conditions to arc jet test conditions requires understanding the evolution of the flight environment and then selecting a combination of test geometries and test conditions to meet a specific test objective [87]. The entry vehicle surface is covered with TPS and the conditions vary spatially. In addition, the condition at any given point will vary with time as well as during the deceleration phase. A comprehensive flight like TPS test will require test capability to vary in time for any given body point. This is not achievable or practical. Instead, for a given TPS, and for a given mission, from the analysis of the flight environment, critical conditions are peak heat flux, peak stagnation pressures and peak shear. A test series may be constructed to ensure that the TPS

material can withstand a combination of these conditions. These tests can be performed with a combination of stagnation coupons and wedges.

This is illustrated in Figure 3.35, the time evolution of heat flux and pressure for a capsule is depicted on the bottom left plot for a non-stagnation body point. At entry heat flux and pressure are zero, and as the capsule start to decelerate, the heat flux and pressure start to rise (follow the arrow) and peak heat flux is achieved first and then the heat flux starts to drop when the stagnation pressure reaches a peak. Further deceleration brings down both the heat flux and pressure. Similarly, the progression of heat flux and shear at the same point is shown in the top left picture. While a stagnation test article could be used to test at critical points, a wedge test article offers a way to test at conditions that may combine heat flux, pressure, and shear. It is challenging to vary test conditions during the test and typical arc jet tests are performed at a fixed condition for a set period of time to capture the ablation and thermal behavior.

Figure 3.35. The conditions vary spatially as well as temporally at any given point on the surface of flight vehicle. The standard test geometries in the arc jet are either stagnation or wedge geometries. The conditions achievable in the arc jet using these articles can only match a limited sub-set of flight quantities. Typically, maximum heat flux and pressure could be matched using stagnation test article. Wedge article may match peak shear at some relevant pressure or heat flux but not all three.

Arc jet testing is also useful for screening (comparative testing) TPS materials, for developing material thermal performance prediction models, and for exploring material or system performance limit (failure). Typically, thermal performance modeling related tests are performed with a stagnation coupon integrated with a thermocouple plug. Data are collected at different conditions of heat flux, pressure, and heat-load and the experimental data base is used to develop a thermal response model. For an ablative TPS, tests at high heat flux and pressure conditions will provide recession data and at lower conditions, with minimal or no recession, the effect of pyrolysis and thermal conduction can be measured. These two groups of tests then provide data for developing an ablative thermal response model. Though shear may play a role, as shear is not modeled in the thermal response models, testing under shear conditions and comparing data with predictions allow for verification of the accuracy of the thermal response model. If shear results in

loss of material, due to melt flow or spallation, then the comparison will be poor. In the case of non-ablative TPS, achieving flight relevant surface temperature will be the driving requirement.

Facility heat flux and pressure measurements made with standard calorimeters can help in the selection of facility operating conditions, nozzle and test location. The heat flux anticipated on the actual test geometry have to be inferred or it has to be measured using a calorimeter of the same shape as the test article. Shear is never measured. For the use of a wedge test article shear has to be computed using boundary layer theory or using modern computational fluid dynamic codes.

In the past decade, high fidelity computation fluid dynamic (CFD) methods, successfully used in flight vehicle design, have been applied to modeling arc jet flow [80, 86, 88, 89]. These CFD solvers provide much needed insight into flight as well as facility environment and their capability can be very useful in test article selection, design, and in selecting arc jet test conditions. Hence, using such tools for pre-test design and prediction allows comparison of post-test results.

An example from [88] illustrates the capability of CFD tools. The objective was to select arc jet test conditions relevant for recession dominated region of the flight and demonstrated the predictive capability to model the recession when the shape of the article is changing. The shape change in turn modifies the local heat flux and in turn changes the rate of recession. Hence, the coupling between shape change and recession at the stagnation location of the model was important to model and predict. The test provided a way to validate the modeling approach. Figure 3.36 shows the stagnation coupon in the arc jet. Figure 3.37 shows the CFD modeling and prediction of the arc jet nozzle (from the throat) including the stagnation model. Figure 3.38 shows the thermo-chemical state of the air along the nozzle center line. These finer details are impossible to measure and hence CFD has become a necessary tool in arc jet test design.

Figure 3.36. Arc Jet test article used in the CFD simulation [88].

Figure 3.37. CFD simulation of the arc jet nozzle flow and the blunt-body test article in the test chamber [88].

Figure 3.38. Flow properties along the IHF 13-inch diameter nozzle center line and model stagnation streamline [88].

More complex and flight like geometries can also be tested using CFD. While it is more expensive to design, manufacture and test such articles, they provide a unique advantage over standard stagnation and wedge articles, especially for complex configuration testing or for improving flight to facility traceability.

The example selected illustrates a complex test article involving designing and testing a photographically scaled version of the flight article [90]. The SPRITE article, schematic shown in Figure 3.39 and the actual article in Figure 3.40, was designed with CFD [91] (Figure 3.41) in support of developing a set of complex tools to predict thermal soak problem of a sample return capsule. The objective was to instrument and collect both TPS as well as internal temperature data both during the arc jet test as well as during cool down, after the test, where the internal temperature may rise due to heat-soak. In order to accommodate the large model, the test team had to assure the facility that the model size would not result in flow blockage. This was first done with CFD [91]. Next, a slightly larger wood spherical model was designed with CFD and then tested to provide confidence that CFD predictions can provide confidence in model design. Figure 3.42 shows the picture of the wood article taken during the test along with CFD simulation on the right. The model size did not choke the nozzle flow. More interesting is the predicted separation location matches very well the observed separation location on the back of the wood model. Features, such as separation on the back side was predicted by the CFD simulation prior to arc jet testing.

Figure 3.39. Schematic of the complex arc jet test article in support of Sample Return Missions [90].

Figure 3.40. Sting mounted test article in the arc jet prior to testing [90].

Figure 3.41. Pre-test prediction for a large test article [91].

Figure 3.42. Wood blockage model during the arc jet test (left) and the pre-test computational prediction (right) [91].

Use of CFD to design complex test article are more prevalent now than ever. The following additional examples illustrate both the power of the CFD as well as arc jet testing. The C-PICA test article shown on the left side of Figure 3.43 was developed for comparison testing of a new

conformal TPS similar to PICA with standard PICA [92]. C-PICA was used in the nose region where peak heat flux and pressure will cause maximum recession. Three of the four segments around the nose were made of C-PICA and one was made of standard PICA. All of the segments were instrumented. This one test provided data for a combination of heat flux, pressure, and shear at two different conditions and provided performance of C-PICA on three panels, and also data on PICA to compare with.

Figure 3.43. Examples of complex arc jet test articles. C-PICA on the left and ADEPT carbon fabric system on the right.

The test article on the right side of Figure 3.43 is a new deployable heat shield concept [93]. It uses stitched carbon fabric draped over ribs and stretched (like an umbrella). This complex configuration was a scaled down version of a flight test article and provided conditions on the entire surface similar to the flight vehicle. It showed a complex heating pattern that was predicted before the test, using our CFD solvers, providing confidence in our ability to predict flight environment.

List of Figures

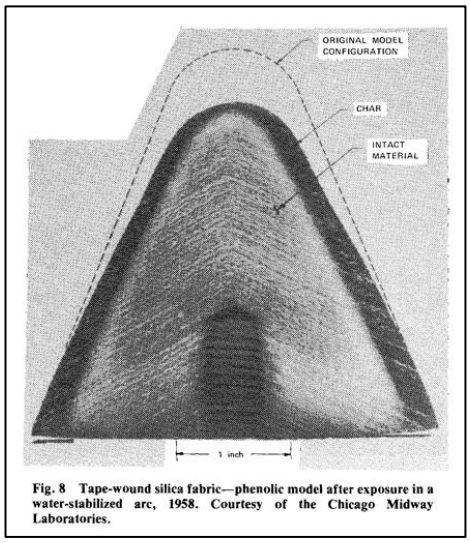

Fig. 8 Tape-wound silica fabric—phenolic model after exposure in a water-stabilized arc, 1958. Courtesy of the Chicago Midway Laboratories.

Fig. 3.17. The above figure from Ref [70] shows one of the earliest (1958) ablative TPS, silica-phenolic, post-test article tested in the arc jet by the Chicago Midway Laboratories. One can observe the tape wrapped material from the x-ray image and also the threaded screw at the bottom. Variant of silica-phenolic ablative TPS materials were used later in DoD ballistic missiles and on NASA's Mercury mission.

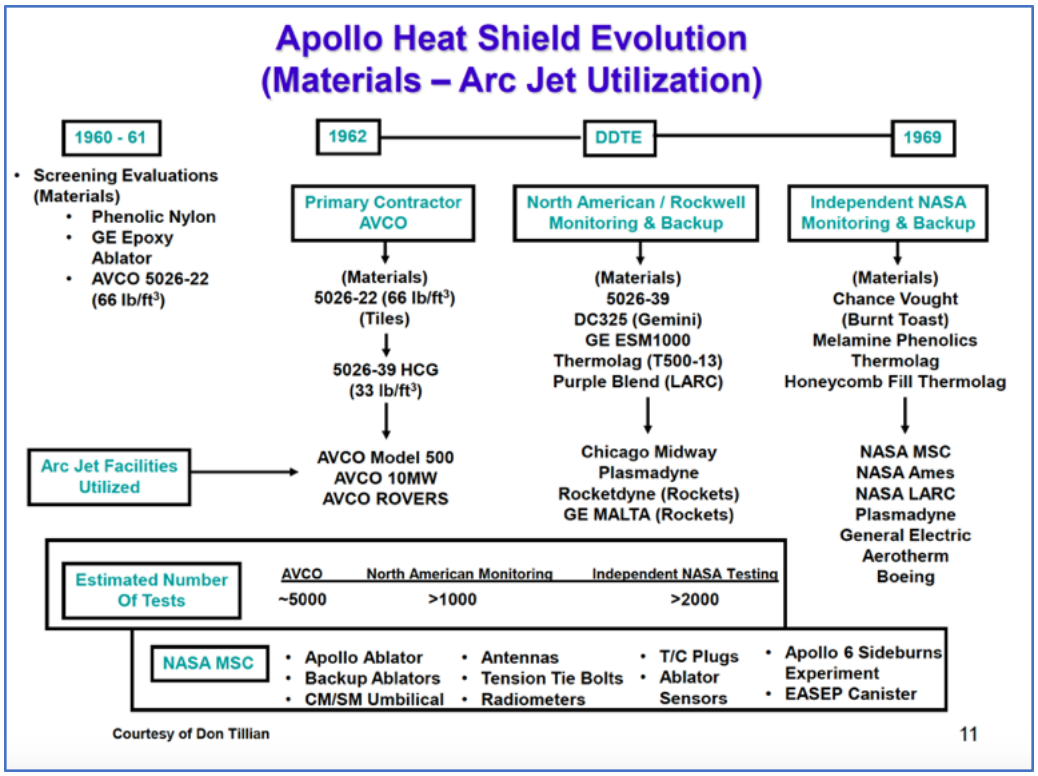

Figure 3.18. More than 10,000 arc jet tests were performed across a variety of arc jets located across the US in the development of TPS for the Apollo program [71].

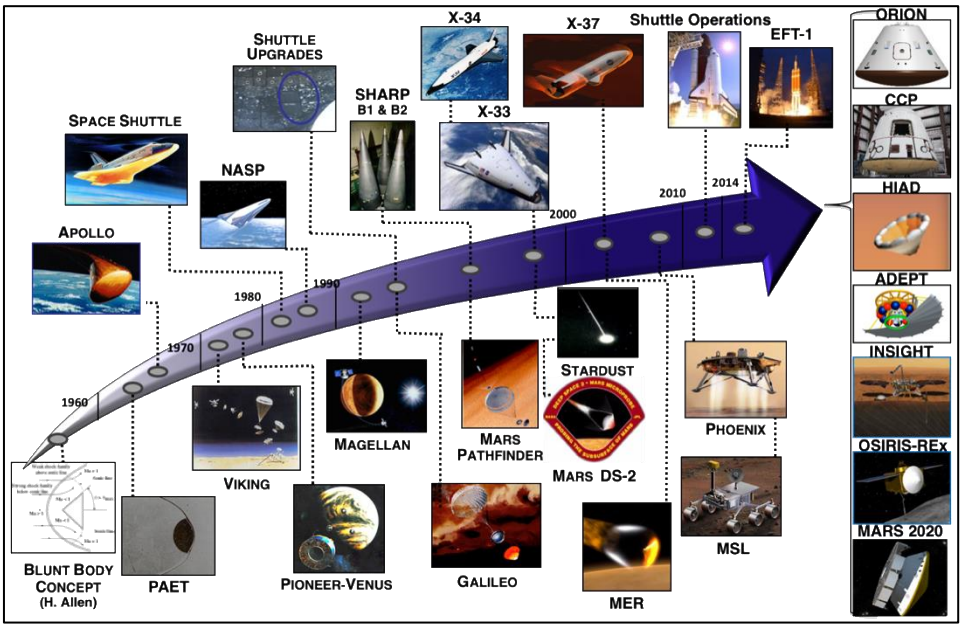

Fig. 3.19. NASA Missions, from the 60's through present, that utilized arc jet in their TPS development (Courtesy of NASA Ames Research Center).

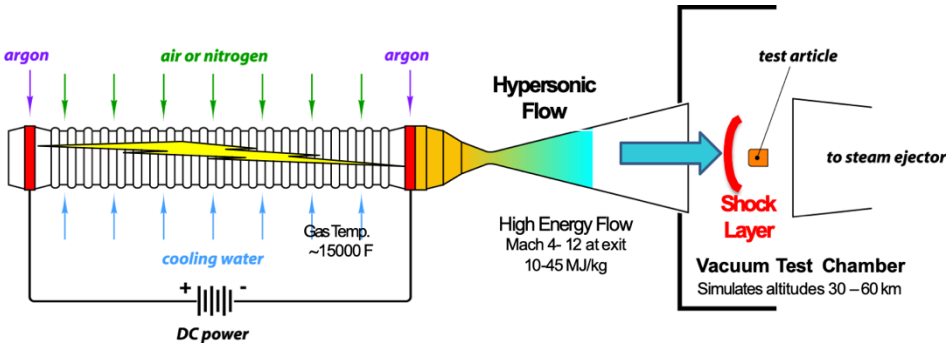

Figure 3.20. A schematic of the 60 MW segmented arc jet used in the Interacting Heating Facility (IHF) at NASA Ames Research Center [73].

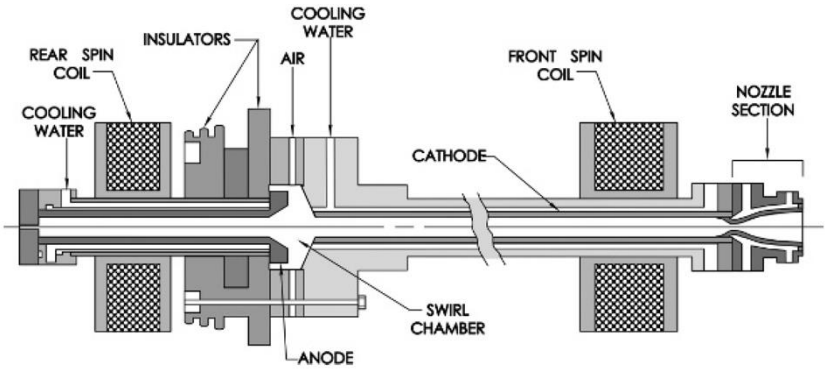

Figure 3.21. Schematic of Huels arc heater design used in the H2 facility at AEDC [74].

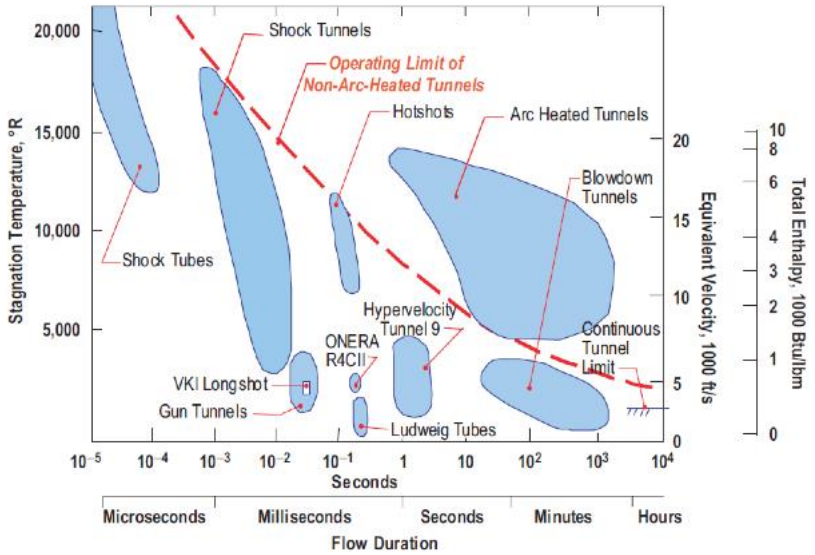

Figure 3.22. Comparison of high-temperature test facilities in terms of stagnation temperature and test duration [73].

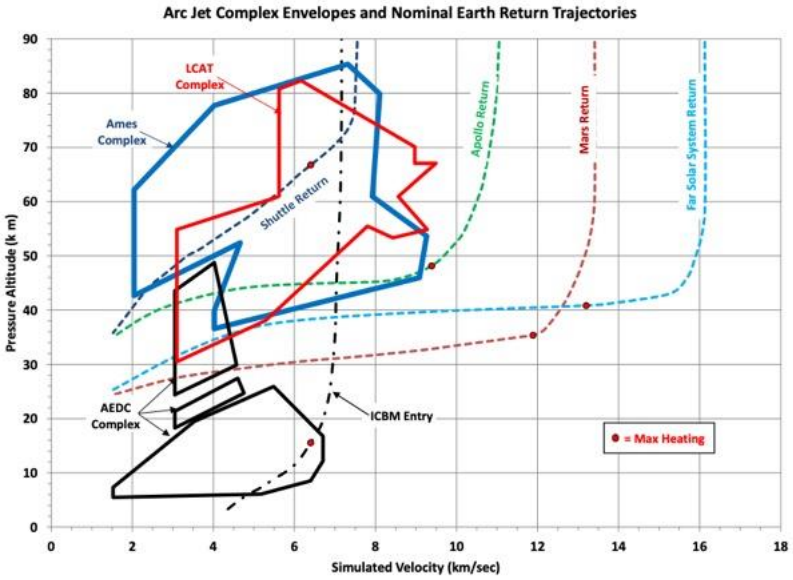

Figure 3.23. Re-entry trajectory and the peak heating conditions for ICBM, Space Shuttle Orbiter, Apollo, Mars, and Far Solar System missions are compared to the NASA Ames, Boeing LCAT, and AEDC arc jet complex operational envelope [73].

Figure 3.24. NASA Ames Arc Jet Complex, supported by a common infrastructure that occupied (2 – 3) city block, consists of Aerodynamic Heating Facility (AHF), Interaction Heating Facility (IFH)), Panel Test Facility (PTF), and Turbulent Facility (TFD) [72].

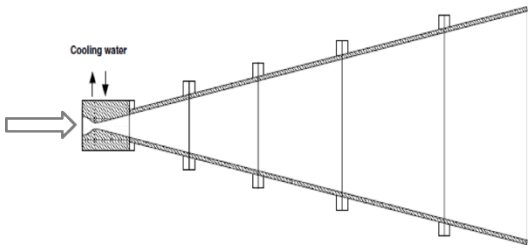

Figure 3.25. Nozzle extensions are often used to expand the flow from to achieve lower test condition with larger test articles in a given arc jet facility [72].

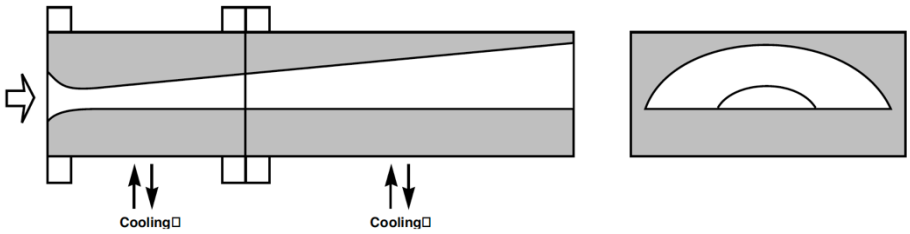

Figure 3.26. Schematic Drawing of a semielliptical nozzle used at NASA ARC [72].

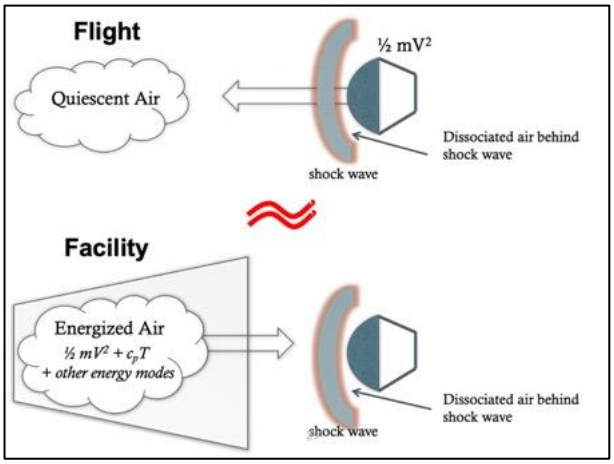

Figure 3.27. A simplified view of the relationship between flight and facility.

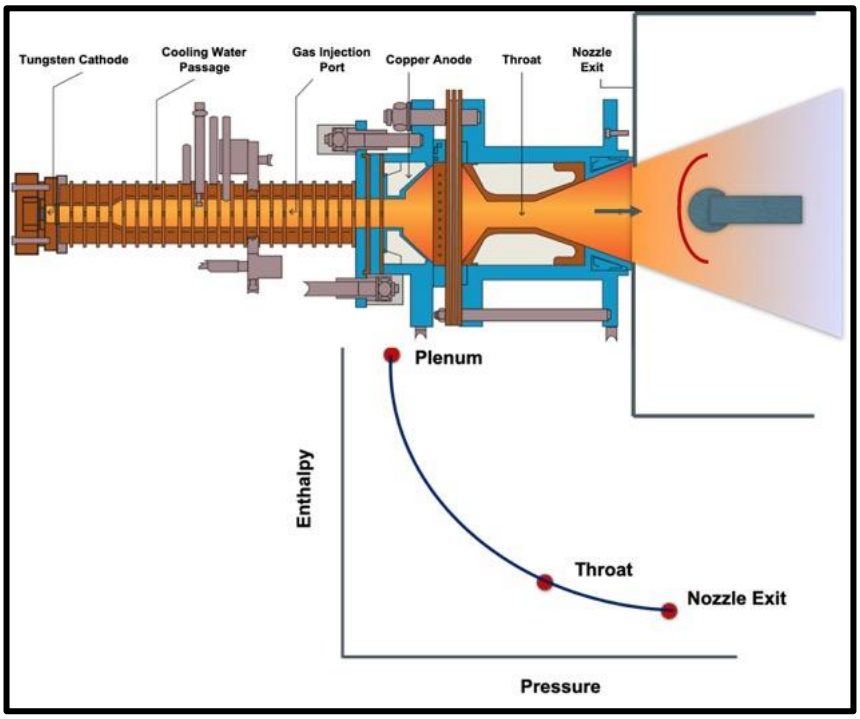

Figure 3.28. The center-line enthalpy and the pressure profile.

(a) Hemisphere ((b) Iso-q (c) Flat-faced cylinder

(d) Null point

Figure 3.29. Standard calorimeters, (a) Hemi-sphere, (b) Iso-q, (c) Flat-face cylinders and (d) Null point calorimeters. A small copper slug (or Gardon gauge) is located at the center of each of the first three oxygen free copper calorimeters. The null point calorimeter has a very small (and quick

time response) heat-sensing element at the tip of the hemisphere-cone body made of oxygen free copper. The sensing element of the null point calorimeter is actually flat [80].

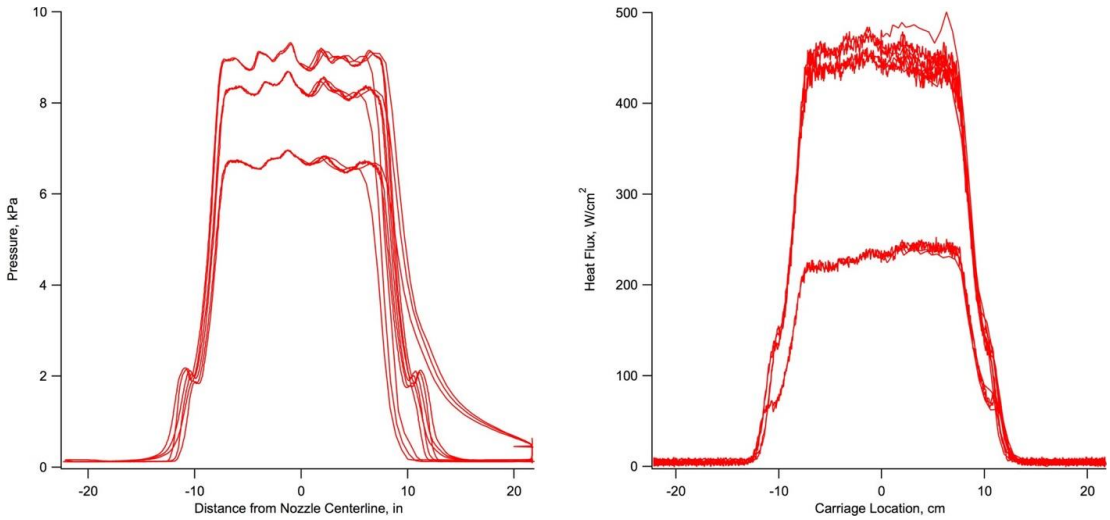

Figure 3.30. Profiles of heat flux and pitot pressure obtained by sweeping 5/8-inch hemisphere-cylinder probes across the jet of the AHF 18-inch axisymmetric nozzle for various arc-heater conditions. The probes were swept at an axial location of 10 inches from the nozzle exit plane. The pitot pressure and heat flux traces show small variations in what can otherwise be considered an uniform distribution (Figures and caption from [80]).

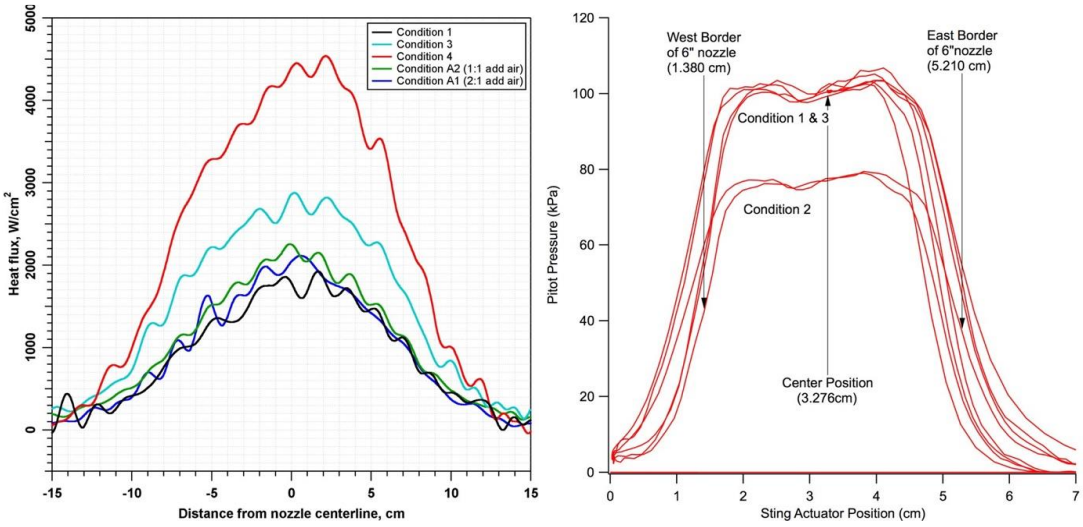

Figure 3.31. Profiles of heat flux and pitot pressure obtained by sweeping a null point calorimeter, and a 5/8-inch hemisphere-cylinder probe, respectively, across the jet of the IHF 6-inch nozzle for various arc-heater conditions. The probes were swept at an axial location of 3 inches from the nozzle exit plane. While the pitot pressure traces show essentially uniform pressure across the jet, the heat flux traces show distinct profiles. Assuming the effective radius of the null point probe does not vary across the jet, one can conclude that profiles of total enthalpy have the same shape as the heat flux. (Figure and caption from [80]).

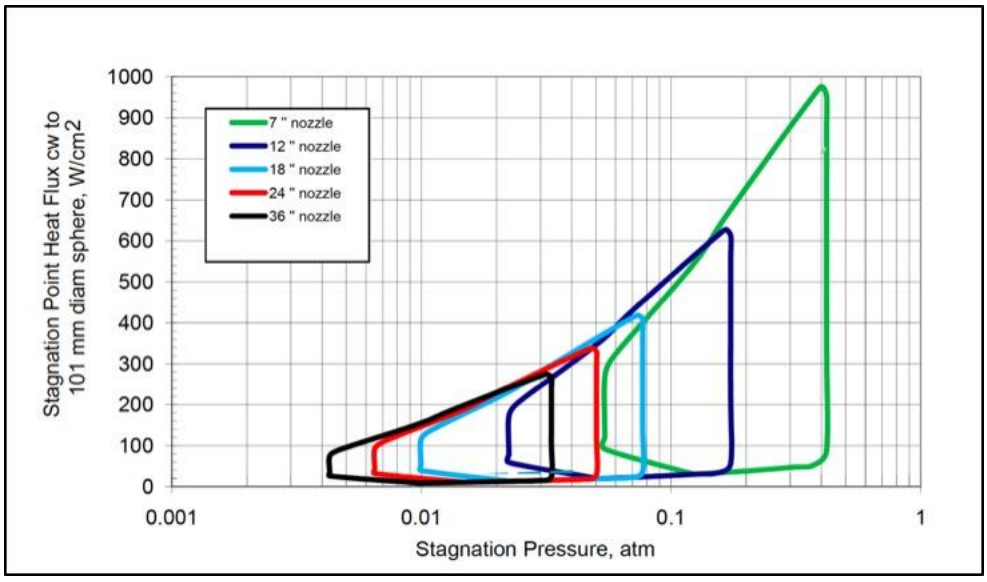

Figure 3.32. Operating envelope of the AHF with 20-MW segmented arc heater [72].

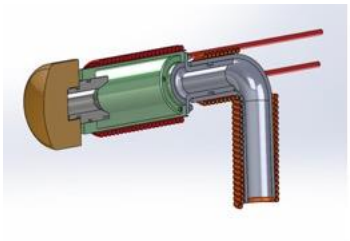

Cut-away view of AHF sting with stagnation model

Typical test setup in the AHF with 5 sting arms (5 test articles)

Typical test setup in the IHF limited to 2 sting arms

Figure 3.33. The test article model holder and the typical test set-up in NASA's AHF and IHF arc jet facilities.

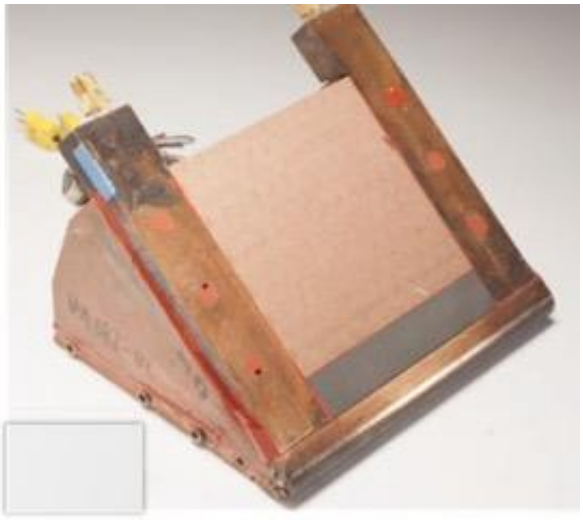

Figure 3.34. An example of a wedge test article used in early Crew Exploration Vehicle (CEV) and in MSL TPS testing [85].

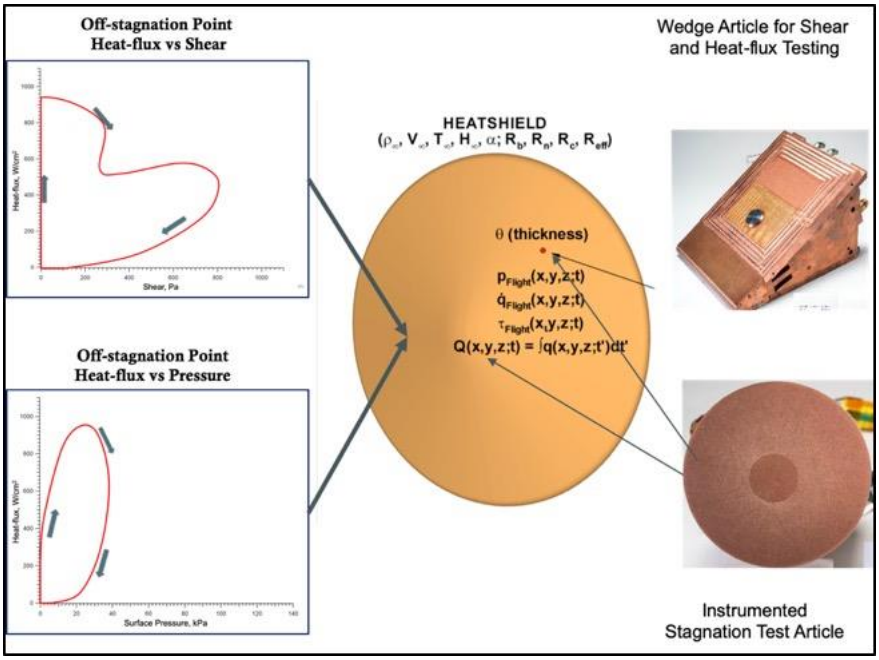

Figure 3.35. The conditions vary spatially as well as temporally at any given point on the surface of flight vehicle. The standard test geometries in the arc jet are either stagnation or wedge

geometries. The conditions achievable in the arc jet using these articles can only match a limited sub-set of flight quantities. Typically, maximum heat flux and pressure could be matched using stagnation test article. Wedge article may match peak shear at some relevant pressure or heat flux but not all three.

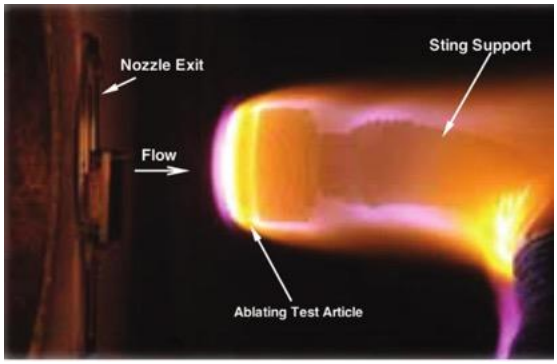

Figure 3.36. Arc Jet test article used in the CFD simulation [88].

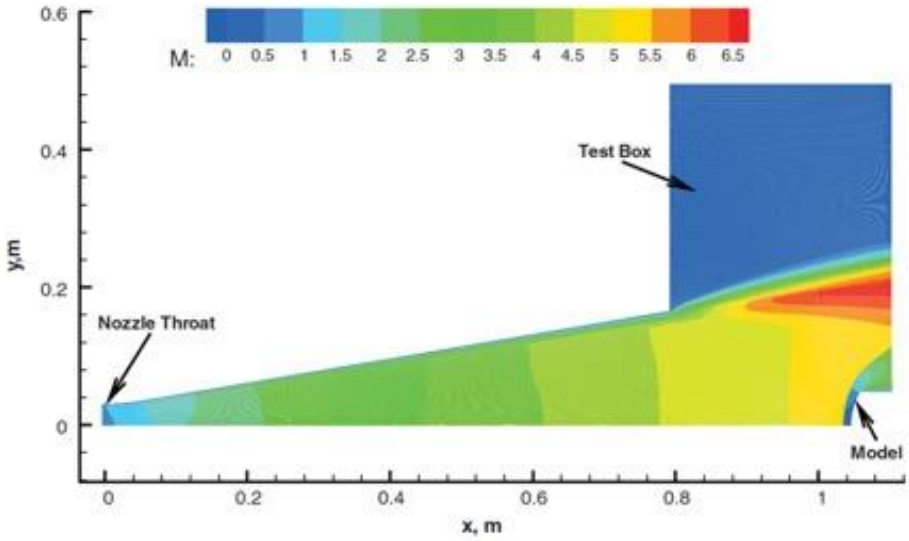

Figure 3.37. CFD simulation of the arc jet nozzle flow and the blunt-body test article in the test chamber [88].

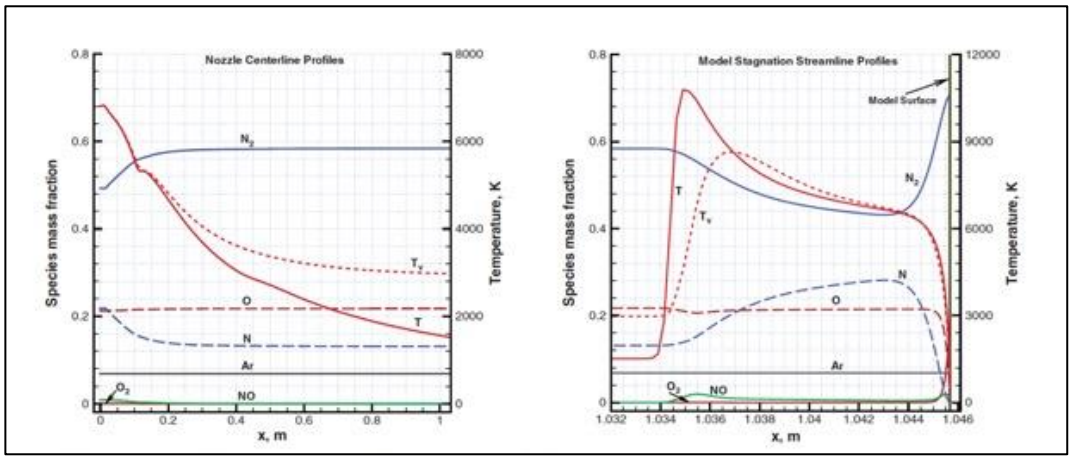

Figure 3.38. Flow properties along the IHF 13-inch diameter nozzle center line and model stagnation streamline [88].

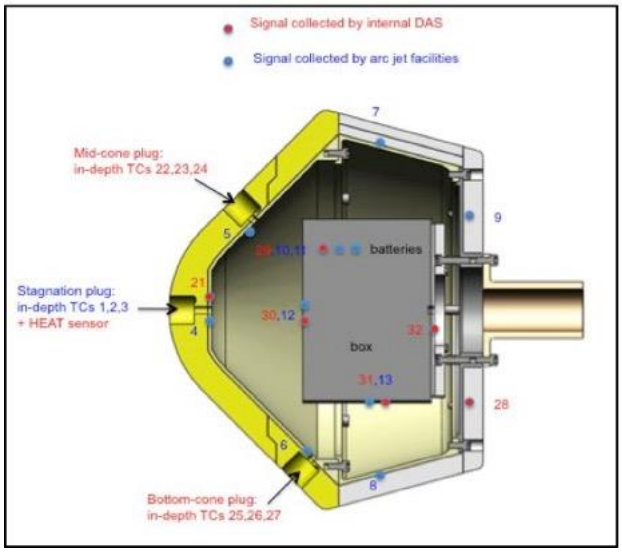

Figure 3.39. Schematic of the complex arc jet test article in support of Sample Return Missions [90].

Figure 3.40. Sting mounted test article in the arc jet prior to testing [90].

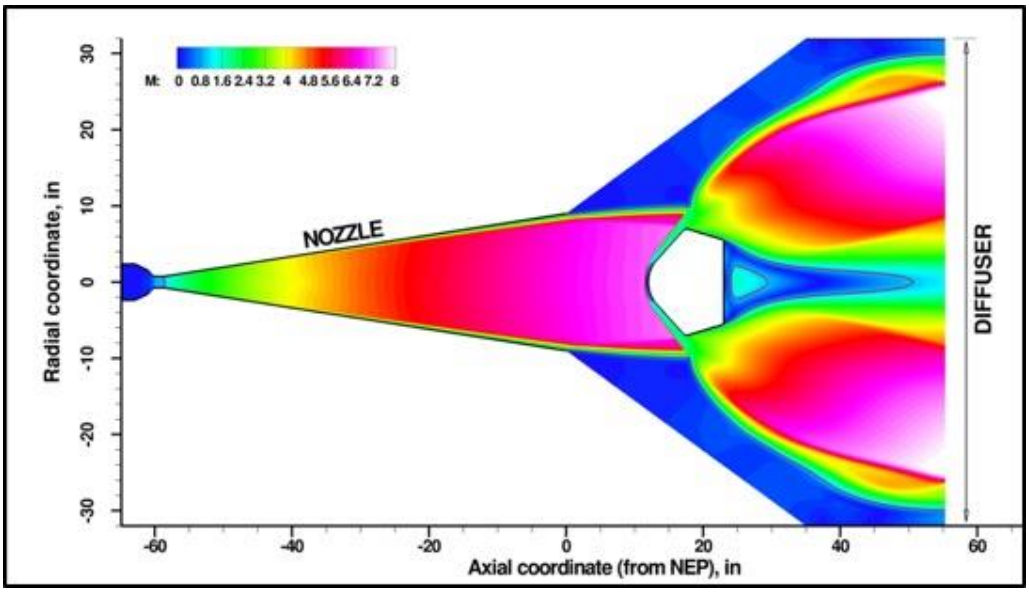

Figure 3.41. Pre-test prediction for a large test article [91].

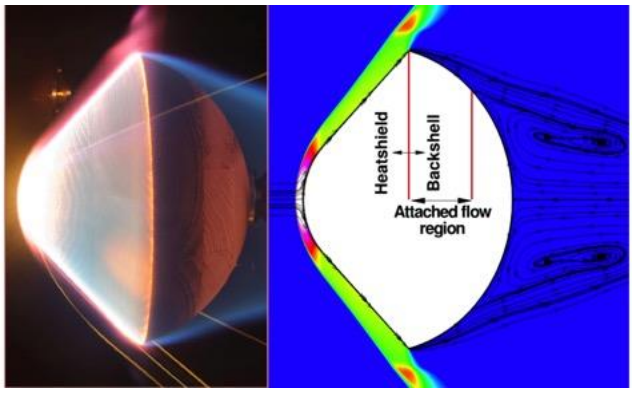

Figure 3.42. Wood blockage model during the arc jet test (left) and the pre-test computational prediction (right) [91].

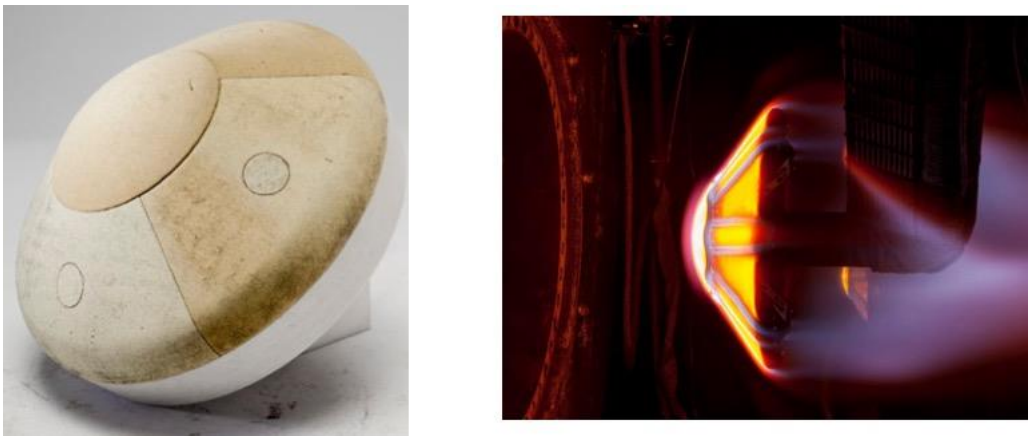

Figure 3.43. Examples of complex arc jet test articles. C-PICA on the left and ADEPT carbon fabric system on the right.

List of Tables

Table 3.5. *NASA Ames Arc Jet Test Facilities Conditions [78]*

Facility	Feature	Gas	Input Power (MW)	Nozzle Exit (inches)	Bulk Enthalpy (MJ/kg)	Surface Pressure (atm)	Convective Heating Rates* (W/cm²)
AHF	Laminar flow	Air N_2	20	Conical 12, 18, 24, 30, 36	10 - 32	0.005 - 0.125 0.0001 - 0.001	20 - 225, 0.05 - 22
AHF/TP3	Separate gas injection	O_2 N_2	10	Conical 5, 7.5, 10, 15	6 - 46	0.1 - 0.5 0.001 – 0.02	0.6 - 1500 0.5 - 250
IHF	Laminar flow	Air	60	Conical 3, 6,13,21,30,41 Semi-elliptical 8 x 32	7 - 47	0.010 - 6.0, 0.0001 - 0.02	50 - 6000, 0.5 - 45
IHF/LEAF **	Laser plus arc flow	Air	60	Conical 9 Semi-elliptical 8 x 32	7 - 47	0.010 - 1.2 0.0001 - 0.02	200 - 1100, 25 - 150
PTF	Laminar panel flow	Air	20	Semielliptical 4 x 17	5 - 32	0.0006 - 0.3	0.5 - 250
Turbulent Flow Duct	Turbulent channel flow	Air N_2	12	2 x 9 Channel	3.5 – 11	0.02 - 0.15	2 - 65

*Heating rate shown above are for a cold wall, fully catalytic value on a 4-inch diameter hemisphere.

**LEAF performance parameters are design estimates.

Table 3.6. *AEDC Arc Jet Test Facilities Conditions [79]*

Facility Name	HEAT-H1	HEAT-H2	HEAT-H3
Facility Type	**Atm. Exhaust (Freejet)**	**Subatm. Exhaust**	**Atm. Exhaust (Freejet)**
Maximum Run Time (minute)	1-2	3-30	1-2
Nozzle Mach Number	1.8 to 3.5	3.4 to 8.3	1.8 to 3.5
Nozzle Exit Diamater (inches)	0.75 to 3.0	5.0 to 24.0	1.2 to 4.5
Stagnation Pressure (atm)	Up to 100	Up to 12	Up to 115
Stagnation Enthalpy* (Btu/lbm)	600-8,500	1,200-5,500	600-8,500
Mass Flow Rate (lbm/sec)	0.5-8	2-10	3-25
Facility Power (NW)	Up to 30	Up to 45	Up to 70

*Stagnation enthalpy inferred from stagnation heat flux and pressure measurements by the Fay-Ridell method.

3.10. References

1. Favaloro, M., *Ablative Materials*, in *Kirk-Othmer Encyclopedia of Chemical Technology*. 2000, Wiley.
2. Rallini, M., M. Natali, and L. Torre, *Chapter 14 - An Introduction to Ablative Materials and High-Temperature Testing Protocols*, in *Nanomaterials in Rocket Propulsion Systems*, Q.-L. Yan, et al., Editors. 2019, Elsevier. p. 529-549.
3. Schmidt, D.L. and H.S. Schwartz, *Evaluation methods for ablative plastics. A review of the techniques used.* Polymer Engineering & Science, 1963. **3**(4): p. 238-250.
4. Aghaaliakbari, B., A. Jafari Jaid, and M.A.A. Zeinali, *Computational Simulation of Ablation Phenomena in Glass-filled Phenolic Composites %J Iranian Journal of Chemistry and Chemical Engineering (IJCCE).* 2015. **34**(1): p. 97-106.
5. Bottin, B., et al., *The VKI plasmatron characteristics and performance*. 2000, VON KARMAN INST FOR FLUID DYNAMICS RHODE-SAINT-GENESE (BELGIUM).
6. Pulci, G., et al., *Carbon–phenolic ablative materials for re-entry space vehicles: Manufacturing and properties.* Composites Part A: Applied Science and Manufacturing, 2010. **41**(10): p. 1483-1490.
7. Natali, M., et al., *A nanostructured ablative bulk molding compound: development and characterization.* Composites Part A: Applied Science and Manufacturing, 2011. **42**(9): p. 1197-1204.
8. Miller-Oana, M., et al., *Oxidation Behavior of Aerospace Materials in High Enthalpy Flows Using an Oxyacetylene Torch Facility.* 2015. **98**(4): p. 1300-1307.
9. Allcorn, E., et al., *Development of an experimental apparatus for ablative nanocomposites testing*, in *47th AIAA/ASME/SAE/ASEE Joint Propulsion Conference & Exhibit*. 2011. p. 6050.
10. Gutierrez, L.G., et al. *Design of small-scale ablative testing apparatus with sample position and velocity control*. in *56th AIAA/ASCE/AHS/ASC Structures, Structural Dynamics, and Materials Conference*. 2015.
11. ASTM, *E457-08, Standard test method for measuring heat-transfer rate using a thermal capacitance (Slug) calorimeter*, in *Annual book of ASTM standards, Space simulation; aerospace and aircraft; Compos. mater*. 2008. p. 15.
12. Lee, J., et al., *Heating rate and nanoparticle loading effects on thermoplastic polyurethane elastomer nanocomposite kinetics*, in *41st AIAA Thermophysics Conference*. 2009, AIAA. p. 4096.
13. Lee, J.C., J.H. Koo, and O.A. Ezekoye, *Thermoplastic polyurethane elastomer nanocomposites: Density, hardness, and flammability properties correlations*, in *AIAA Paper*. 2009.
14. Koo, J.H., et al., *Flammability studies of a novel class of thermoplastic elastomer nanocomposites.* Journal of fire sciences, 2010. **28**(1): p. 49-85.
15. Lee, J.C.-S., *Characterization of ablative properties of thermoplastic polyurethane elastomer nanocomposites*, in *Dept. of Mechanical Engineering*. 2010, The University of Texas at Austin: Austin, TX.
16. Lee, J., J. Koo, and O. Ezekoye, *Thermoplastic polyurethane elastomer nanocomposite ablatives: Characterization and performance*, in *47th AIAA/ASME/SAE/ASEE Joint Propulsion Conference & Exhibit*. 2011, AIAA: San Diego, CA. p. 6051.

17. Schellhase, K.J., et al., *Experimental Characterization of Material Properties of Novel Silica/Polysiloxane Ablative.* Journal of Spacecraft and Rockets, 2018. **55**(6): p. 1401-1413.
18. Natali, M., et al., *In-situ Ablation Recession Sensor Based on Ultra-Miniature Thermocouples-Part A: 0.25 mm Diameter Thermocouples*, in *49th AIAA/ASME/SAE/ASEE Joint PropulsionConference*. 2013. p. 3660.
19. Yee, C., et al., *In Situ Ablation Recession Sensor for Ablative Materials Based on Ultraminiature Thermocouples.* Journal of Spacecraft and Rockets, 2014. **51**(6): p. 1789-1796.
20. Koo, J.H., et al., *In Situ Ablation Recession and Thermal Sensor for Thermal Protection Systems.* Journal of Spacecraft and Rockets, 2018. **55**(4): p. 783-796.
21. Ewing, M.E., T.S. Laker, and D.T. Walker, *Numerical Modeling of Ablation Heat Transfer.* Journal of Thermophysics and Heat Transfer, 2013. **27**(4): p. 615-632.
22. Salazar, G., et al., *Development and Verification of Enclosure Radiation Capabilities in the CHarring Ablator Response (CHAR) code*, in *46th AIAA Thermophysics Conference*. 2016, American Institute of Aeronautics and Astronautics: Washington, DC.
23. Amar, A.J., et al., *Overview of the CHarring Ablator Response (CHAR) Code*, in *46th AIAA Thermophysics Conference*. 2016, American Institute of Aeronautics and Astronautics: Washington, DC.
24. Oliver, B. and A.J. Amar, *Inverse Heat Conduction Methods in the CHAR Code for Aerothermal Flight Data Reconstruction*, in *46th AIAA Thermophysics Conference*. 2016, American Institute of Aeronautics and Astronautics.
25. Koo, J.H. and T. Mensah, *Novel Polymer Nanocomposite Ablative Technologies for Thermal Protection of Propulsion and Reentry System for Space Application*, in *Nanotechnology Commercialization: Manufacturing Processes and Products*, T. Mensah, et al., Editors. 2018, Wiley & Sons: New York, NY. p. 177-244.
26. Lisco, B., et al., *Insitu Ablation and Thermal Sensing of a 3D Carbon/Phenolic Composite for Computer Modeling and Simulation*, in *58th AIAA/ASCE/AHS/ASC Structures, Structural Dynamics, and Materials Conference*. 2017. p. 0356.
27. Menz, R., et al., *Characterization of 3-D Woven Carbon/Phenolic using In-Situ Ablation Sensing, Video Imaging, and Numerical Simulation*, in *2018 AIAA/ASCE/AHS/ASC Structures, Structural Dynamics, and Materials Conference*. 2018. p. 0098.
28. Chaboki, A., et al., *Supersonic torch facility for ablative testing*, in *5th Joint Thermophysics and Heat Transfer Conference*. 1990, AIAA, Reston, VA.
29. Koo, J.H., et al., *A Cost-Effective Approach to Evaluate High-Temperature Ablatives for Military Applications.* Naval Engineers Journal, 1992. **104**(3): p. 166-177.
30. Yang, B.C., F.B. Cheung, and J.H. Koo, *Modeling of One-Dimensional Thermomechanical Erosion of High-Temperature Ablatives.* Journal of Applied Mechanics, 1993. **60**(4): p. 1027-1032.
31. Wilson, D., D. Beckley, and J. Koo. *Development of new materials for missile launch structures*. in *JANNAF Propulsion Meeting*. 1993.
32. Cheung, F., et al. *Effect of melt layer formation on thermo-mechanical erosion of high-temperature ablative materials*. in *PICAST'1 1993- Pacific International Conference on Aerospace Science and Technology, National Cheng Kung University, Tainan, Taiwan*. 1993.

33. Zanetti, M., G. Camino, and R. Mulhaupt, *Combustion behavior of EVA/Flourohectprote nanocomposites.* Polym. Degrad. Stab., 2001. **74**: p. 413-417.
34. Yang, B.C., F.B. Cheung, and J.H. Koo, *Numerical investigation of thermo-chemical and mechanical erosion of ablative materials*, in *29th Joint Propulsion Conference and Exhibit*. 1993, AIAA.
35. Miller, M., et al., *Effect of reinforcements in a silicone resin composite*, in *32nd Aerospace Sciences Meeting and Exhibit*. 1994, AIAA.
36. Koo, J., et al., *Performance envelope of a silicone polymer composite.* Moving Forward With 50 Years of Leadership in Advanced Materials., 1994. **39**: p. 1576-1589.
37. VanMeter, M., et al. *Mechanical properties and material behavior of a glass silicone polymer composite*. in *INTERNATIONAL SAMPE SYMPOSIUM AND EXHIBITION*. 1995. SAMPE SOCIETY FOR THE ADVANCEMENT OF MATERIAL.
38. Cheung, F. and J. Koo, *Prediction of Thermo-mechanical Erosion of High-Temperature Ablatives in the SSRM Facility*. 1995, AIAA-95-0254, 33rd Aerospace Sciences Meeting, Reno, NV, AIAA, Reston, VA.
39. Koo, J., et al. *Effects of major constituents on the performance of silicone polymer composite*. in *Proceedings of the 1998 30th International SAMPE Technical Conference*. 1998. SAMPE.
40. Koo, J., et al. *Silicone matrix composites for thermal protection*. in *Proceedings of the 1999 31st International SAMPE Technical Conference:'Advanced Materials and Processes Preparing for the New Millennium'*. 1999.
41. Koo, J.H., et al. *Nanocomposite rocket ablative materials: processing, characterization, and performance*. in *International SAMPE Symposium and Exhibition (Proceedings)*. 2003. Soc. for the Advancement of Material and Process Engineering.
42. Koo, J., et al., *Nanostructured materials for rocket propulsion system: recent progress*, in *44th AIAA/ASME/ASCE/AHS/ASC Structures, Structural Dynamics, and Materials Conference*. 2003. p. 1769.
43. Koo, J., et al., *Nanocomposite rocket ablative materials: processing, microstructure, and performance*, in *45th AIAA/ASME/ASCE/AHS/ASC Structures, Structural Dynamics & Materials Conference*. 2004. p. 1996.
44. Koo, J.H. and L.A. Pilato, *Polymer nanostructured materials for high temperature applications.* Sampe Journal, 2005. **41**(2): p. 7-19.
45. Koo, J.H., *Polymer nanocomposites: Processing, Characterization, and Applications*. 1st ed. 2006, New York, NY: McGraw-Hill Professional Pub.
46. Koo, J.H., et al., *Silicone Polymer Composites for Thermal Protection System: Fiber Reinforcements, Microstructures, and Performance*, in *45th AIAA/ASME/SAE/ASEE Joint Propulsion Conference & Exhibit*. 2009, AIAA.
47. Koo, J.H., et al., *Silicone polymer composites for thermal protection system: fiber reinforcements and microstructures.* Journal of Composite Materials, 2010. **45**(13): p. 1363-1380.
48. Koo, J.H., et al., *Silicone Polymer Composites for Thermal Protection of Naval Launching System.* Journal of Spacecraft and Rockets, 2011. **48**(6): p. 904-919.
49. Koo, J.H., et al. *Nanocomposite rocket ablative materials: Subscale ablation test*. in *SAMPE 2004*. 2004. SAMPE.
50. Koo, J.H., L.A. Pilato, and G.E. Wissler, *Polymer nanostructured materials for propulsion systems.* Journal of spacecraft and rockets, 2007. **44**(6): p. 1250-1262.

51. Blanski, R., et al. *Polymer nanostructured materials for solid rocket motor insulation-ablation performance*. in *52nd JANNAF Propulsion Meeting,*. 2004. Las Vegas, NV: CPIAC, Columbia, MD.
52. Ruth, P., R. Blanski, and J.H. Koo. *Preparation of polymer nanostructured materials for solid rocket motor insulation*. in *Proc. 52nd JANNAF Propulsion Meeting*. 2004. Las Vegas, NV: CPIAC, Columbia, MD.
53. Koo, J.H., et al. *Polymer nanostructured materials for solid rocket motor insulation–processing, microstructure, and mechanical properties*. in *52nd JANNAF Propulsion Meeting*. 2004. Las Vegas: CPIAC, Columbia, MD.
54. McDermott, R., et al. *Advanced Thermal Protection System Composite using Needle Punched Silica Fabrics*. in *2018 CAMX*. 2018. Dallas, TX: SAMPE, Covina, CA.
55. Hull, R. and M. Lander, *Laser hardened materials evaluation laboratory (LHMEL)*. Journal of Laser Applications, 1996. **8**(3): p. 161-168.
56. Sepka, S., et al., *Testing of Candidate Rigid Heat Shield Materials at LHMEL for the Entry, Descent, and Landing Technology Development Project*, in *Advanced Ceramic Coatings and Materials for Extreme Environments II*. 2012. p. 127-155.
57. Petry, J. and R.J. Hull. *LHMEL Laser/Materials Interaction Testing*. 2017 [cited 2019 19th May 2019]; Available from: https://www.wpafb.af.mil/Portals/60/documents/T2/2017_0143%20Tri-Fold%20RX%20Facility%20CRADA%20brochures_Basic%20LHMEL.PDF?ver=2017-10-26-121811-207.
58. Lander, M.L., et al. *Laser-Hardened Materials Evaluation Laboratory testing facility*. in *Laser-Induced Damage in Optical Materials: 1991*. 1992. International Society for Optics and Photonics.
59. Bottin, B., et al. *The VKI 1.2 MW Plasmatron facility for the thermal testing of TPS materials*. in *3rd European Workshop on Thermal Protection Systems, ESA-ESTEC*. 1998.
60. Chazot, O., J. Pereira Gomes, and M. Carbonaro, *Characterization of a'mini-plasmatron'facility by pitot probe measurements*, in *29th AIAA, Plasmadynamics and Lasers Conference*. 1998. p. 2478.
61. Owens, W., et al., *Development of a 30kw inductively coupled plasma torch for aerospace material testing*, in *10th AIAA/ASME Joint Thermophysics and Heat Transfer Conference*. 2010. p. 4322.
62. Greene, B.R., et al., *Characterization of a 50kW Inductively Coupled Plasma Torch for Testing of Ablative Thermal Protection Materials*, in *55th AIAA Aerospace Sciences Meeting*. 2017, American Institute of Aeronautics and Astronautics.
63. Bottin, B., et al., *A decade of aerothermal plasma research at the von Karman Institute*. Contributions to plasma physics, 2004. **44**(5-6): p. 472-477.
64. Bottin, B., et al. *Experimental and computational determination of the VKI Plasmatron operating envelope*. in *30th Plasmadynamic and Lasers Conference*. 1999.
65. Anderson Jr, J.D., *Hypersonic and high-temperature gas dynamics*. 2006: American Institute of Aeronautics and Astronautics.
66. *LR1504 Prepreg datasheet. Website: http://www.lewcott.com/ablatives.html*.
67. Swenson, L.S., C.C. Alexander, and J.M. Grimwood, *This new ocean: a history of Project Mercury*. Vol. 4201. 1966: Scientific and Technical Information Division, Office of Technology ….

68. Allen, H.J. and A.J. Eggers Jr, *A study of the motion and aerodynamic heating of ballistic missiles entering the earth's atmosphere at high supersonic speeds*. 1958: NACA.
69. Hacker, B.C. and J.M. Grimwood, *On the Shoulders of Titans: a history of Project Gemini*. Vol. 4203. 1977: National Aeronautics and Space Administration.
70. Sutton, G.W., *The initial development of ablation heat protection, an historical perspective.* Journal of Spacecraft and Rockets, 1982. **19**(1): p. 3-11.
71. Curry, D.M., *Space shuttle orbiter thermal protection system design and flight experience.* 1993.
72. Terrazas-Salinas, I.e.a., *Test Planning Guide for NASA Ames Research Center Arc Jet Complex and Range Complex*, T.F. Branch, Editor. 2018, NASA Ames Research Center: Space Technology Division, NASA Ames Research Center, Moffett Field, CA.
73. Calomino, A., et al., *Evaluation of the NASA Arc Jet Capabilities to Support Mission Requirements*. 2010, NASA.
74. Hammock, G., *Arc Heater Capability Upgrade at AEDC.* ITEC Journal, 2010.
75. Marren, D. and F. Lu, *Advanced hypersonic test facilities*. 2002: American Institute of Aeronautics and Astronautics.
76. *Test Facility Guide, Arnold Engineering Development Complex (AEDC)*, in *Advanced Hypersonic Test Facilities*. 2017: AEDC, Arnold AFB, TN.
77. Splinter, S., et al. *Comparative Measurements of Earth and Martian Entry Environments in the NASA Langley HYMETS Facility*. in *49th AIAA Aerospace Sciences Meeting including the New Horizons Forum and Aerospace Exposition*. 2011.
78. Raiche, *Private Communication*. 2019, NASA Ames Reserach Center: NASA Ames Reserach Center.
79. *Fact sheet-High-Enthalpy Arc-Heated Facilities at AEDC*. 2013, AEDC: Arnold AFB, TN. p. 1380.
80. Prabhu, D., et al. *CFD Analysis Framework for Arc-Heated Flowfields I: Stagnation Testing in Arc jets at NASA ARC*. in *41st AIAA Thermophysics Conference*. 2009.
81. Fay, J.A., *Theory of stagnation point heat transfer in dissociated air*. Journal of the Aerospace Sciences, 1958. **25**(2): p. 73-85.
82. Pope, R.B., *Stagnation-point convective heat transfer in frozen boundary layers.* AiAA journal, 1968. **6**(4): p. 619-626.
83. Zoby, E.V., *Empirical stagnation-point heat-transfer relation in several gas mixtures at high enthalpy levels*. 1968, NASA.
84. Fletcher, D.G., *Measurement requirements for improved modeling of arcjet facility flows*. 2000, NATIONAL AERONAUTICS AND SPACE ADMINISTRATION MOFFETT FIELD CA AMES ….
85. Terrazas-Salinas, I., et al. *Comparison of heat transfer measurement devices in arc jet flows with shear*. in *10th AIAA/ASME Joint Thermophysics and Heat Transfer Conference*. 2010.
86. Prabhu, D., et al. *CFD Analysis Framework for Arc-Heated Flowfields II: Shear Testing in Arc jets at NASA ARC*. in *41st AIAA Thermophysics Conference*. 2009.
87. Bose, D., et al. *Ground-to-flight traceability analysis of arcjet testing for the crew exploration vehicle*. in *41st AIAA Thermophysics Conference*. 2009.
88. Gökçen, T., et al. *Applications of CFD Analysis in Arc jet Testing of RCC Plug Repairs*. in *25th AIAA Aerodynamic Measurement Technology and Ground Testing Conference*. 2006.
89. Gokcen, T., K. Skokova, and A. Alunni. *Computational Simulations of Panel Test Facility Flow: Compression-Pad Arc jet Tests*. in *42nd AIAA Thermophysics Conference*. 2011.

90. Agrawal, P., D. Prabhu, and Y.-K. Chen. *Thermal Analysis of Small Re-entry Probes*. in *50th AIAA Aerospace Sciences Meeting including the New Horizons Forum and Aerospace Exposition*. 2012.
91. Prabhu, D. *Flowfield Analysis of a Small Entry Probe (SPRITE) Tested in an Arc Jet*. in *50th AIAA Aerospace Sciences Meeting Including the New Horizons Forum and Aerospace Exposition*. 2012.
92. Milos, F.S., M.J. Gasch, and D.K. Prabhu, *Conformal phenolic impregnated carbon ablator arcjet testing, ablation, and thermal response.* Journal of Spacecraft and Rockets, 2015. **52**(3): p. 804-812.
93. Cassell, A., et al., *System level aerothermal testing for the Adaptive Deployable Entry and Placement Technology (ADEPT).* 2016.
94. Shimoda, T. and K. Yamada. *Arc Heating Wind Tunnel Facility in ISAS/Japan and the activity to update and improve it for Further Sample Return Missions*. 2016. 46th International Conference on Environmental Systems.